A "Mix and Match" Ionic−Covalent Strategy for Self-Assembly of Inorganic Multilayer Films

Mingming Fang, David M. Kaschak, Anthony C. Sutorik, and Thomas E. Mallouk*

Contribution from the Department of Chemistry, The Pennsylvania State University, University Park, Pennsylvania 16802

Received July 28, 1997[⊗]

Abstract: Multilayer thin films consisting of anionic α-zirconium phosphate (α-ZrP) sheets, tetrameric zirconium hydroxide cations $[Zr_4(OH)_8(H_2O)_{16}]^{8+}$ (Zr_4^{8+}), and alkanediylbis(phosphonic acid) (C_nBPA) have been grown on silicon and gold surfaces by sequential adsorption reactions. The thin films were characterized by ellipsometry, X-ray diffraction, reflectance infrared spectroscopy, X-ray photoelectron spectroscopy (XPS), and atomic force microscopy (AFM). Alternately dipping cationic substrates into exfoliated α-ZrP-containing suspensions, aqueous zirconium oxychloride, and ethanolic $C_{16}BPA$ solutions generates a mixed ionic/covalent multilayer structure. The tetrameric Zr_4^{8+} cation adsorbs onto the α-ZrP surface, providing a covalent anchoring point for the growth of the $C_{16}BPA$ layer. Adsorbing a second layer of zirconium ions onto the $C_{16}BPA$ layer allows one to continue the layer growth sequence using either covalent (metal/phosphonate) or ionic (α-ZrP/polycation) interlayer connections. A multilayer film with a repeating α-ZrP/Zr_4^{8+}/$C_{16}BPA$/Zr_4^{8+} sequence is sufficiently well-ordered in the stacking direction to give a Bragg peak in the diffraction pattern. The intensities of infrared absorbances in the symmetric and asymmetric C−H stretching regions, which arise from $C_{16}BPA$, are linear with the $C_{16}BPA$ layer number. This "mix and match" approach provides a versatile means of assembling multilayer heterostructures from both ionic and covalent building blocks, with essentially any desired sequence of layers.

Molecular self-assembly is one of the simplest and most effective methods for preparing thin films.[1] Compared with other film-growth techniques, such as spin coating, laser ablation, sol-gel processing, electroplating, and chemical vapor deposition, self-assembly provides better control of structure at the molecular level. Self-assembled thin films are therefore useful vehicles for studying a variety of surface chemical phenomena on both flat and curved surfaces. They are of interest as interfacial models and in potential applications in many surface-related technologies, including catalysis, chemical sensing, microelectronics, corrosion inhibition, adhesion, and tribology.[2]

While the self-assembly of organic monolayers is now a well-understood process,[1c] the preparation of stable and ordered multilayer films remains a challenge, and relatively few approaches to it have been demonstrated. Most of these involve linking of sequentially grown self-assembled monolayers through covalent[3−5] or noncovalent[6,7] interactions. Inorganic materials are particularly interesting in this regard, because a full range of interlayer bonding schemes (covalent,[4,8] coordinate covalent,[5] and ionic[9−12]) has been demonstrated, and many different kinds of materials (metal phosphates, oxides, colloidal metal particles, coordination networks, intercalation compounds) have been grown as ultrathin films.

In general, covalent multilayer assembly methods provide the finest degree of structural control. For example, one can prepare in this way assemblies of aligned nonlinear optical chromophores,[13] thin films containing well-defined molecule size

[⊗] Abstract published in *Advance ACS Abstracts,* December 1, 1997.

(1) (a) Bard, A. J. *Integrated Chemical Systems*; John Wiley & Sons: New York, 1994. (b) Ulman, A. *An introduction to Ultrathin Organic Films: From Langmuir−Blodgett to Self-Assembly*; Harcourt Brace Jovanovich: Boston, 1991. (c) Ozin, G. A. *Adv. Mater.* **1992**, *4*, 612. (d) Mann, S. *J. Mater. Chem.* **1995**, *5*, 935.

(2) (a) Fendler, J. H. *Membrane Mimetic Approach to Advanced Materials*; Springer-Verlag: Berlin, 1992. (b) Somorjai, G. A. *Chemistry in Two Dimensions: Surfaces*; Cornell University Press: Ithaca, NY, 1981. (c) Noyota, T.; Poling, G. W. *Corrosion* **1979**, *35*, 193. (d) Kepley, L. J.; Crook, R. M.; Ricco, A, *J. Anal. Chem.* **1992**, *64*, 3191.

(3) (a) Netzer, L.; Sagiv, J. *J. Am. Chem. Soc.* **1983**, *105*, 674. (b) Evans, S. D.; Ulman, A.; Goppert-Berarducci, K. E.; Gerenser, L. J. *J. Am. Chem. Soc.* **1991**, *113*, 5866. (c) Cao, G.; Hong, H.-G.; Mallouk, T. E. *Acc. Chem. Res.* **1992**, *25*, 420. (d) Thompson, M. E. *Chem. Mater.* **1994**, *8*, 1168. (e) Katz, H. E. *Chem. Mater.* **1994**, *6*, 2227

(4) (a) Lee, H.; Kepley, L. J.; Hong, H.-G.; Mallouk, T. E. *J. Am. Chem. Soc.* **1988**, *110*, 618. (b) Lee, H.; Kepley, L. J.; Hong, H.-G.; Akhter, S.; Mallouk, T. E. *J. Phys. Chem.* **1988**, *92*, 2597. (c) Akhter, S.; Lee, H.-G.; Mallouk, T. E.; White, J. M. *J. Vac. Sci. Technol. A* **1989**, *7*, 1608. (d) Cao, G.; Hong, H.-G.; Mallouk, T. E. *Acc. Chem. Res.* **1992**, *25*, 420. (e) Yang, H. C.; Aoki, K.; Hong, H.-G.; Sackett, D. D.; Arendt, M. F.; Yau, S.-L.; Bell, C. M.; Mallouk, T. E. *J. Am. Chem. Soc.* **1993**, *115*, 11855. (f) Katz, H. E.; Schilling, M. L.; Chidsey, C. E. D.; Putvinski, T. M.; Hutton, R. S. *Chem. Mater.* **1991**, *3*, 699. (g) Byrd, H.; Pike, J. K.; Talham, D. R.; *Thin Solid Film* **1994**, *244*, 768.

(5) (a) Bell, C. M.; Arendt, M. F.; Gomez, L.; Schmehl, R. H.; Mallouk, T. E. *J. Am. Chem. Soc.* **1994**, *116*, 8374. (b) Bell, C. M.; Keller, S. M.; Lynch, V. M.; Mallouk, T. E. *Mater. Chem. Phys.* **1993**, *35*, 225. (c) Ansell, M. A.; Zeppenfeld, A. C.; Yoshimoto, K.; Cogan, E. B.; Page, C. J. *Chem. Mater.* **1996**, *8*, 591.

(6) (a) Sun, L.; Kepley, L. J.; Crooks, R. M. *Langmuir* **1992**, *8*, 2101. (b) Arias, F.; Godinez, L. A.; Wilson, S. R.; Kaifer, A. E.; Echegoyen, L. *J. Am. Chem. Soc.* **1996**, *118*, 6086.

(7) (a) Decher, G.; Hong, J.-D. *Makromol. Chem., Macromol. Symp.* **1991**, *46*, 321. (b) Decher, G.; Hong, J. D. *Ber. Bunsenges. Phys. Chem.* **1991**, *95*, 1430. (c) Decher, G.; Hong, J.-D.; Schmitt, J. *Thin Solid Films* **1992**, *210/211*, 831. (d) Decher, G. In *Comprehensive Supramolecular Chemistry*; Sauvage, J.-P., Hosseini, M. W., Eds.; Elsevier: Oxford, UK, 1996; Vol. 9, pp 507−528. (e) Lehr, B.; Seufert, M.; Wenz, G.; Decher, G. *Supramol. Sci.* **1995**, *2*, 199. (f) Schmitt, J.; Decher, G.; Dressick, W. J.; Brandow, S. L.; Geer, R. E.; Shashidhar, R.; Calvert, J. M. *Adv. Mater.* **1997**, *9*, 61.

(8) (a) Ichinose, I.; Senzu, H.; Kunitake, T. *Chem. Lett.* **1996**, 831. (b) Ichinose, I.; Senzu, H.; Kunitake, T. *Chem. Mater.* **1997**, *9*, 1296.

(9) (a) Keller, S. W.; Kim, H. N.; Mallouk, T. E. *J. Am. Chem. Soc.* **1994**, *116*, 8817. (b) Feldheim, D. L.; Grabar, K. C.; Natan, M. J.; Mallouk, T. E. *J. Am. Chem. Soc.* **1996**, *118*, 7640. (c) Kim, H. N.; Keller, S. W.; Mallouk, T. E.; Schmitt, J.; Decher, G. *Chem. Mater.* **1997**, *9*, 1414.

(10) (a) Kleinfeld, E. R.; Ferguson, G. S. *Science* **1994**, *265*, 370. (b) Ferguson, G. S.; Kleinfeld, E. R. *Adv. Mater.* **1995**, *7*, 414.

(11) Kotov, N. A.; Dekany, I.; Fendler, J. H. *Adv. Mater.* **1996**, *8*, 637.

(12) (a) Lvov, Y.; Hass, H.; Decher, G.; Möhwald, H. *Langmuir* **1994**, *10*, 4232. (b) Lvov, Y.; Ariga, K.; Kunitake, T. *Chem. Lett.* **1994**, 2323. (c) Lvov, Y.; Ariga, K.; Kunitake, T. *J. Am. Chem. Soc.* **1995**, *117*, 6117. (d) Ichinose, I.; Fujiyoshi, K.; Mizuki, S.; Lvov, Y.; Kunitake, T. *Chem. Lett.* **1996**, 257. (e) Isayama, M.; Nomiyama, K.; Kunitake, T. *Adv. Mater.* **1996**, *8(8)*, 641.

voids for chemical sensing,[14] and ordered multilayers that act as templates for their own replication.[15] The technique does have some important drawbacks, most notably the requirement for specific functional groups and limitations on the lateral area occupied by a given molecule. On the other hand, multilayers joined by ionic contacts are more easily prepared, because specific functional groups or metal—ligand interactions are not required. Ionic multilayers are also very forgiving with respect to the size of molecules that can be included in the layer growth process. A drawback of the ionic method, at least with organic polyelectrolytes, is that there is significant interpenetration of sequentially grown layers. This problem can be eliminated by using certain inorganic sheets as polyanions;[16] still, it is not easy to control molecular orientation or intermolecular distances to the extent possible with covalent multilayer films.

In this paper we describe a "mix and match" strategy that allows one to switch between ionic and covalent interlayer connections within a multilayer adsorption sequence. The technique employs well-characterized covalent and ionic components (zirconium phosphonates and α-Zr(HPO$_4$)$_2$·H$_2$O/poly-(allylamine hydrochloride) (α-ZrP/PAH)), which are themselves compatible with many other covalent and ionic materials. Metal-phosphonate sequential adsorption has previously been used to prepare covalent multilayers with different sequences of divalent, trivalent, or tetravalent metal ions and phosphonates; likewise, α-ZrP as a lamellar colloid can be combined with a very wide variety of organic and inorganic polyelectrolytes.[17] Hence we can anticipate that the "mix and match" method will enable the preparation of self-assembled films from numerous ionic and covalent components. In this paper we demonstrate this idea, and use surface-sensitive techniques (ellipsometry, surface infrared spectroscopy, X-ray diffraction, X-ray photoelectron spectroscopy, and atomic force microscopy) to characterize some representative mixed ionic/covalent multilayer films in detail.

Experimental Section

Materials. Zirconium oxychloride octahydrate (ZrOCl$_2$·8H$_2$O, 99.99%), hafnium oxychloride octahydrate (HfOCl$_2$·8H$_2$O, 99.99+%), and tetrabutylammonium hydroxide (TBA$^+$OH$^-$, 40 wt % solution in water) were obtained from Aldrich and used as received. (4-Aminobutyl)dimethylmethoxysilane (4-ABDMMS), from United Chemical Technologies, Inc. and 2-mercaptoethylamine hydrochloride (2-MEA) from Sigma Chemical Co. were also used as received. All other chemicals were reagent grade and were obtained from commercial sources.

Crystalline α-zirconium phosphate (α-ZrP) was prepared hydrothermally in aqueous HF, as described by Alberti et al.,[18] and its phase purity was confirmed by X-ray powder diffraction. Hexadecanediylbis-(phosphonic acid), H$_2$O$_3$P(CH$_2$)$_{16}$PO$_3$H$_2$ (C$_{16}$BPA), was prepared by the Michaelis—Arbuzov reaction of Br(CH$_2$)$_{16}$Br (Karl Industries, Inc.) and triethyl phosphite. Br(CH$_2$)$_{16}$Br (20 mmol) and P(OC$_2$H$_5$)$_3$ (50 mmol) were refluxed at 150 °C for 6 h, the solution was cooled to room temperature, and about 30 mL of concentrated (36.5—38.0%) aqueous HCl was added. Heating was resumed at 100 °C overnight (16 h). The solution was cooled to room temperature, 10 mL of water was added, and the aqueous layer was then separated. The aqueous phase

was evaporated in air at room temperature for ca. 2 days, and the white precipitate of C$_{16}$BPA was washed several times with HPLC grade CH$_3$-CN and dried in vacuo.

Substrate Preparation. Polished (100) Si wafers were sonicated in CCl$_4$ for 15 min and then rinsed with 2-propanol and water. They were then sonicated in a hot piranha solution of concentrated H$_2$SO$_4$ and 30% H$_2$O$_2$ (3:1) *(CAUTION: Piranha solution can react violently with organic compounds)* for 30 min and rinsed with copious amounts of water. The cleaned Si wafers were then rinsed in methanol, 1:1 methanol/toluene, and toluene before the surface priming and monolayer adsorption steps. Au substrates were purchased from EMF Corp. (Ithaca, NY) as a 1000 Å Au film grown on a 50 Å Ti adhesion layer, on 1 × 3 in. glass microscope slides. The Au substrates were sonicated in ethanol for 5 min and in piranha solution for 15 min and rinsed with copious amounts of water.

The cleaned Si wafers were primed with a cationic amine layer by immersion in a 2 wt % 4-ABDMMS/toluene solution under an Ar purge and stored inside a desiccator overnight. After the priming step, the Si wafers were washed twice in toluene, once in 2-propanol, and once in methanol and dried under Ar before used. The cleaned Au substrates were similarly primed with an amine monolayer in a 5 wt % 2-MEA/ethanol solution in air in a cold room (4 °C) for 4 h.

Exfoliation of α-Zr(HPO$_4$)$_2$·H$_2$O (α-ZrP). Colloidal suspensions of α-ZrP were prepared by adding ca. 1.25×10^{-4} mol of TBA$^+$OH$^-$ to 0.05 g (1.66×10^{-4} mol) of microcrystalline α-ZrP in 25 mL of nanopure water. The solution was gently agitated in an ice bath (0 °C) for 1 h before adsorbing the monolayer sheets onto the amine-primed substrates.

Instrumentation and Measurements. Ellipsometric data were obtained on a Gaertner Model L2W26D ellipsometer with a HeNe laser (632.8 nm) light source. The incident angle was 70°, and the polarizer was set at 45°. Typically, the thicknesses of 5—7 spots/sample were measured and averaged. Optical constants were measured values for Au substrates and literature values ($N_s = 3.875$, $K_s = -0.018$) for Si substrates. The real part of the refractive index of the film was fixed at 1.54, which is a typical value for organic materials, and which matched the measured values of films within about 0.1 during measurements. The imaginary part of the film refractive index was assumed to be zero.

Reflectance IR spectra were measured with a Nicolet 730 FT-IR spectrometer, which had a Spectratech Inc. FT-80 film attachment that keeps the angle of incidence fixed at 80°. The optical bench was purged with dry nitrogen, and the spectrometer was equipped with a liquid nitrogen cooled MCT-A detector. Spectra were recorded after 1024 scans at a resolution of 2 cm^{-1} and were referenced to spectra of the unmodified Au substrate. Samples for FT-IR measurements were prepared on 1 × 1 in. Au substrates. X-ray photoelectron spectra (XPS) were obtained with a Hewlett-Packard 5950A spectrometer, which had a Mg Kα line source. The samples were measured at 20° and 75° take-off angles from the surface normal. Survey spectra were performed at a resolution of 1 eV, and quantitative surface compositions were measured by integration of slower scans taken at a resolution of 0.1 eV.

Thin-film X-ray diffraction experiments were performed on a Philips X'Pert MPD powder diffractometer equipped with thin film attachments (collimator, collimator adjustment bracket, and 0.1 mM slit). The low-angle part of the diffraction patterns (Kiessig fringes) was obtained after optimizing the alignment of the incident and reflected beams.

Atomic force microscopy (AFM) was performed with a Digital Nanoscope IIIa system. The pyramidal AFM tips and cantilevers were made from etched silicon probes. All AFM images were collected in tapping mode in air, resonating the tip just below the oscillation frequency of the cantilever (typically 250—325 kHz). The scanning frequency was 1—2 Hz, and the data collection resolution was 512 × 512 pixels. Tips were changed frequently to maintain the resolution of the AFM images.

Results and Discussion

Preparation of Multilayer Ionic/Covalent Self-Assembled Films. Multilayer films were grown by using the adsorption scheme outlined in Figure 1. Cationic substrates (alkylamine-
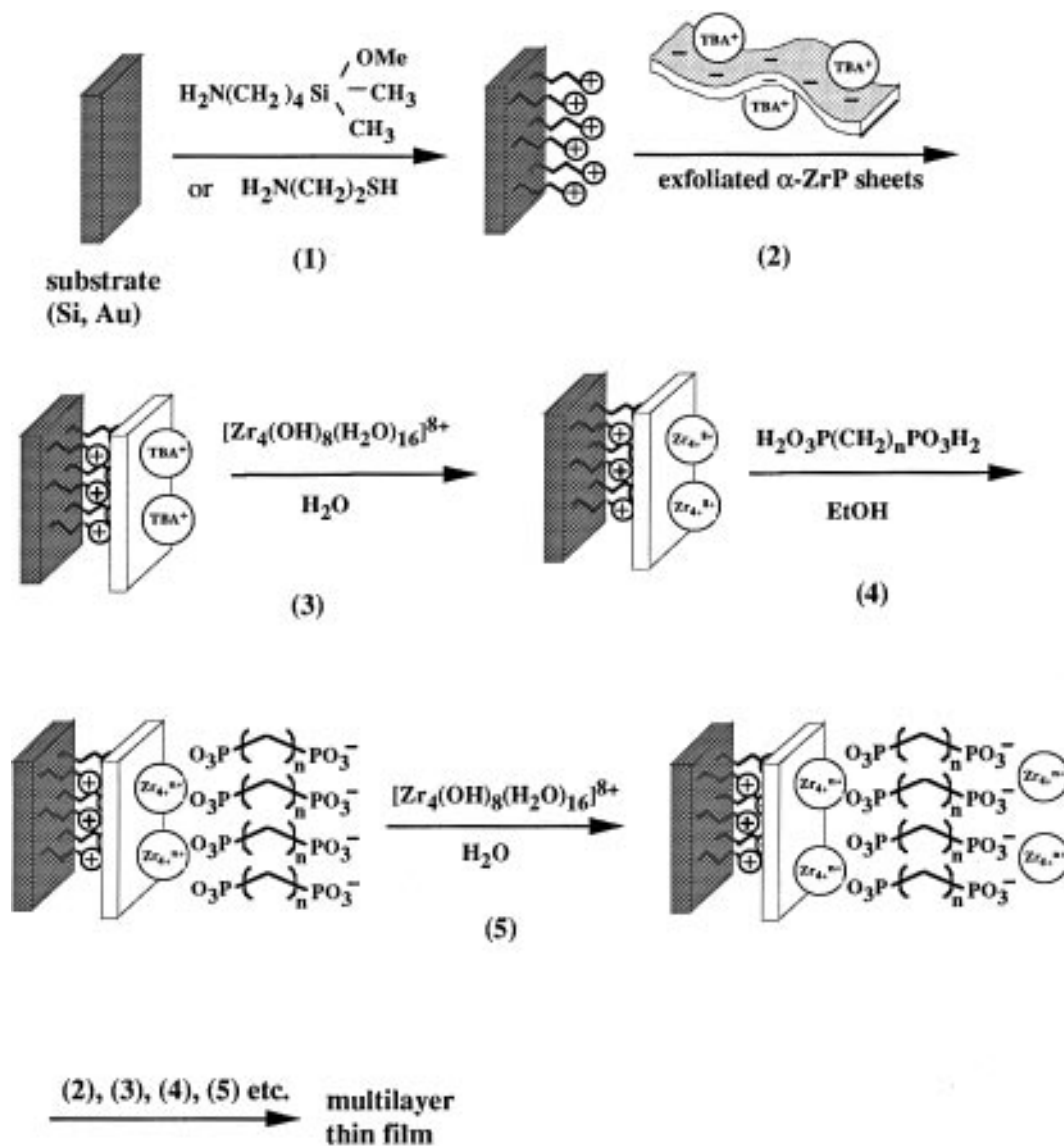
(13) Katz, H. E.; Scheller, G.; Putvinski, T. M.; Schilling, M. L.; Wilson, W. L.; Chidsey, C. E. D. *Science* **1991**, *254*, 1485.

(14) (a) Brousseau, L. C., III; Mallouk, T. E. *Anal. Chem.* **1997**, *69*, 679. (b) Brousseau, L. C., III; Aurentz, D. J.; Benesi, A. J.; Mallouk, T. E. *Anal. Chem.* **1997**, *69*, 688.

(15) Maoz, R.; Matlis, S.; DiMasi, E.; Ocko, B. M.; Sagiv, J. *Nature* **1996**, *384*, 150.

(16) Kaschak, D. M.; Mallouk, T. E. *J. Am. Chem. Soc.* **1996**, *118*, 4222.

(17) Mallouk, T. E.; Kim, H.-N.; Ollivier, P. J.; Keller, S. W. In *Comprehensive Supramolecular Chemistry*; Alberti, G., Bein T., Eds.; Elsevier Press: Oxford, UK, **1996**; Vol. 7, pp 189—218.

(18) Alberti, G.; Torracca, E. *J. Inorg. Nucl. Chem.* **1968**, *30*, 317.

Figure 1. Sequential adsorption scheme for growing α-ZrP/Zr$_4^{8+}$/C$_{16}$BPA/Zr$_4^{8+}$ multilayer films.

derivatized Si and Au) were immersed in a colloidal suspension of α-ZrP sheets. When the unilamellar α-ZrP colloid is placed in contact with an amine-modified surface at a suitable pH (ca. 8.0), surface NH$_3^+$ groups displace the TBA$^+$ on one side of the α-ZrP sheets, which are thus adsorbed as a dense monolayer on the surface.[9]

Normally, the anionic α-ZrP monolayer is used in the ionic self-assembly process to bind the next polycation layer. To switch to covalent layer growth, the α-ZrP-covered surface is immersed in a 5 mM aqueous solution of ZrOCl$_2$·8H$_2$O. In this solution, the predominant form of zirconium is the tetrameric hydroxycation[19] Zr$_4$(OH)$_8$(H$_2$O)$_{16}^{8+}$ (abbreviated Zr$_4^{8+}$), which charge compensates the adsorbed α-ZrP layer. This Zr$_4^{8+}$-terminated surface then binds a monomeric bis(phosphonic acid), such as H$_2$O$_3$P(CH$_2$)$_{16}$PO$_3$H$_2$ (C$_{16}$BPA), from a 10 mM ethanolic solution. Multilayer covalent films can then be grown from an appropriate sequence of metal ion and bis(phosphonic acid) adsorption steps.

To switch back to ionic multilayer growth, the C$_n$BPA-terminated surface is again reacted with an aqueous Zr$_4^{8+}$ solution, and then with the α-ZrP colloid. The shortest "mix

and match" sequence that one can prepare is thus α-ZrP/Zr$_4^{8+}$/C$_n$BPA/Zr$_4^{8+}$/α-ZrP. Repeating sequences of this type ($n = 4$, 8, 10, 12, 14, 16) were grown on silicon and gold substrates, and the $n = 16$ films were studied in greatest detail. "Mix and match" films containing longer covalent (C$_{16}$BPA/Zr^{4+}) and ionic (α-ZrP/PAH) repeats were also prepared and characterized.

Ellipsometry. The stepwise growth of self-assembled multilayer films can be conveniently monitored by ellipsometry. Figure 2a shows a plot of film thickness vs adsorption step for films consisting of the surface priming layer and α-ZrP, and subsequent adsorbed layers of Zr$_4^{8+}$ (1st Zr$_4^{8+}$), C$_{16}$BPA, and Zr$_4^{8+}$ (2nd Zr$_4^{8+}$). The average thickness increase in the deposition of the α-ZrP sheets is 13 Å, which is about 5 Å thicker than expected for the 7.6 Å thick α-ZrP lamellae.[20] On the other hand, the average thickness increase for the 1st Zr$_4^{8+}$ layer is about 4 Å, somewhat smaller than the smallest dimension of this disk-shaped (5 × 9 Å) tetrameric cation.[19a] The discrepancies between the expected and observed thicknesses are too large to be attributed to errors in the assumed optical constants[21] (±10%), and may arise from the loosely bound TBA$^+$ cations, which charge-compensate the anionic α-ZrP surface and are displaced by adsorption of Zr$_4^{8+}$ ions.

(19) (a) Clearfield, A.; Vaughan, P. A. *Acta Crystallogr.* **1956**, *9*, 555. (b) Devia, D. H.; Sykes, A. G. *Inorg. Chem.* **1981**, *20*, 910. (c) Thompson, R. C. *Inorg. Chem.* **1985**, *24*, 3542. (d) Fryer, J. R.; Hutchison, J. L.; Paterson, R. *Nature* **1970**, *226*, 149.

(20) Troup, J. M.; Clearfield, A. *Inorg. Chem.* **1977**, *16*, 3311.
(21) Zeppenfeld, A. C.; Fiddler, S. L.; Ham, W. K.; Kopfenstein, B. J.; Page, C. J. *J. Am. Chem. Soc.* **1994**, *116*, 9158.
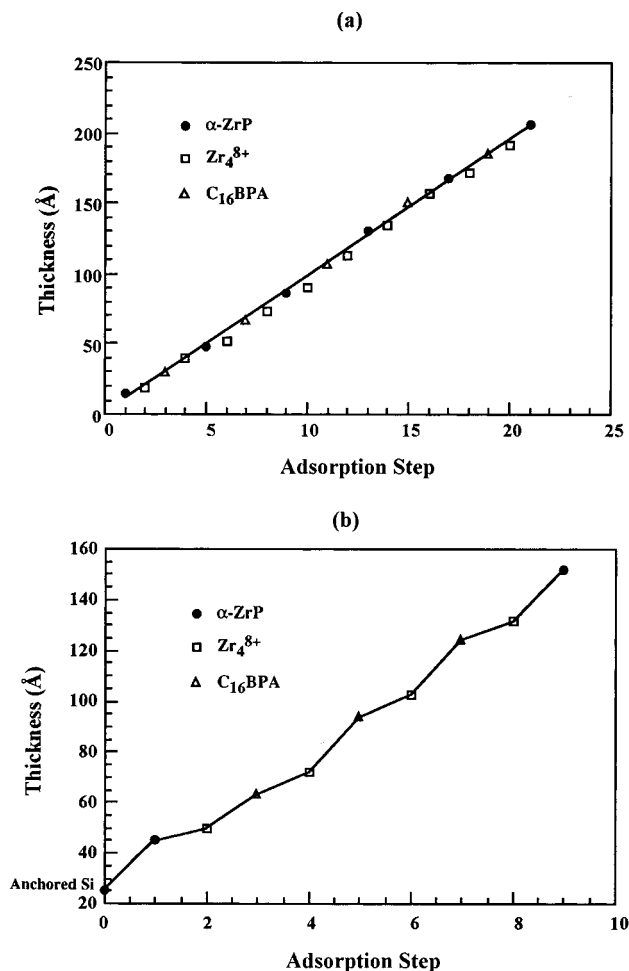
(a)

(b)

Figure 2. (a) Ellipsometric thickness data for α-ZrP/Zr$_4^{8+}$/C$_{16}$BPA/Zr$_4^{8+}$ multilayer films on Si/4-ABDMMS. The solid line represents the best linear fit to the α-ZrP data points, and shows that the average distance between α-ZrP sheets is 39 Å. (b) Ellipsometric thickness data for covalent Zr-C$_{16}$BPA multilayers grown between α-ZrP/Zr$_4^{8+}$ bilayers on Si/4-ABDMMS. In both parts a and b, the time allowed for each adsorption step was 3 h.

The solid line through the α-ZrP data points in Figure 2a shows that the repeating sequence α-ZrP/Zr$_4^{8+}$/C$_{16}$BPA/Zr$_4^{8+}$ corresponds consistently to a 39 Å increase in thickness.

The average thickness increase for the C$_{16}$BPA layer adsorbed onto the Zr$_4^{8+}$-terminated surface is 14 Å, which is much shorter than the 22.5 Å increase expected in a metal-C$_{16}$BPA multilayer film.[4e] However, if layer growth is then continued in the covalent mode (by alternately adsorbing Zr$_4^{8+}$ and C$_{16}$BPA), the average thickness increase for the second and third C$_{16}$-BPA layer is 22 Å (Figure 2b). It appears therefore that the first C$_{16}$BPA layer grows with a greater chain tilt angle, and that subsequent layers revert to the α-zirconium phosphonate structure, with an approximate tilt angle of 31° from the surface normal. The change in structure with layer number is reminiscent of several studies which have shown that the degree of order and packing density in metal phosphonate films is sensitive to the nature of the priming layer.[22,23] In this case, the low density of alkyl chains is probably a consequence of the fact that fewer binding sites are available per unit area on the α-ZrP/Zr$_4^{8+}$ surface than on the C$_n$BPA/Zr$_4^{8+}$ surface. This result suggests that the coverage of the zirconium(IV) species on the
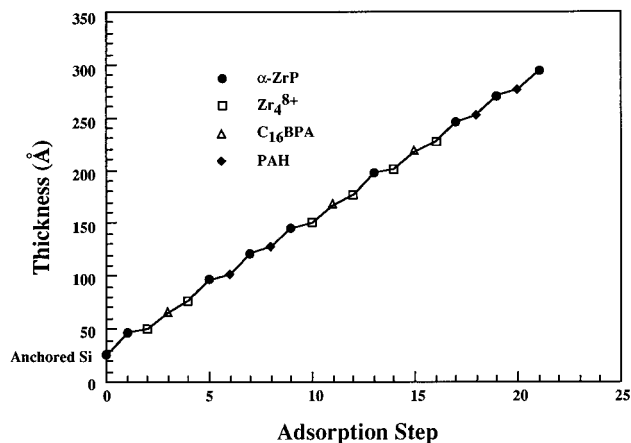
(22) Frey, B. L.; Hanken, D. G.; Corn, R. M. *Langmuir* **1993**, *9*, 1815.
(23) (a) Byrd, H.; Pike, J. K.; Talham, D. R. *Chem. Mater.* **1993**, *5*, 709. (b) Byrd, H.; Whipps, S.; Pike, J. K.; Ma, J.; Nagler, S. E.; Talham, D. R. *J. Am. Chem. Soc.* **1994**, *116*, 295.


Figure 3. Ellipsometric thickness data for α-ZrP/Zr$_4^{8+}$/C$_{16}$BPA/Zr$_4^{8+}$/α-ZrP/PAH heterostructures on Si/4-ABDMMS. The durations of the covalent (Zr$_4^{8+}$ and C$_{16}$BPA) and ionic (α-ZrP and PAH) adsorption steps were 3 h and 15 min, respectively.

two surfaces may be different, a point that is borne out by XPS studies (see below).

The "mix and match" approach is also effective for switching from covalent to ionic layer growth. This point is demonstrated by the ellipsometric data shown in Figure 3. In this case two α-ZrP/PAH layer pairs were inserted into the repeating α-ZrP/Zr$_4^{8+}$/C$_n$BPA/Zr$_4^{8+}$/α-ZrP sequence shown in Figure 2. The thicknesses of ionic layer pairs are consistent with previous data from purely ionic films.[9] The shift back to the covalent sequence again involves an anomalously thin (14 Å) C$_{16}$BPA layer. It is apparent from Figures 2 and 3 that one can switch back and forth several times between ionic and covalent linking, without significant changes in the reproducibility of either the ionic or covalent adsorption sequences.

X-ray Diffraction. X-ray diffraction of the thin films provides similar and complementary information to the ellipsometric data. Bragg diffraction peaks contain information about the lamellar structures and the degree of order of the film along the stacking axis. From the positions of Kiessig fringes in the low-angle part of the diffraction pattern, the total film thickness can be calculated, independent of the refractive index used in the calculation of ellipsometric thickness. An X-ray diffraction pattern of a film containing the simple "mix and match" sequence α-ZrP/Zr$_4^{8+}$/C$_{16}$BPA/Zr$_4^{8+}$ repeated six times on a 4-ABDMMS-primed Si wafer shows a Bragg peak at 2.1° 2θ (Figure 4). This result confirms that the α-ZrP and C$_{16}$-BPA layers are not arranged randomly in the film, but stack along the surface normal as in a lamellar metal phosphonate or ionic intercalation compound. The position of the Bragg peak gives a repeat distance of approximately 41 Å between α-ZrP sheets, which is consistent with the ellipsometric results (average of 39 Å). From the positions of Kiessig fringes in the low-angle part of the diffraction pattern (Figure 4, inset), the total thickness of the film was calculated to be 220 Å, also in good agreement with the ellipsometrically derived thickness of 230 Å.

Infrared Spectra. Multilayer films grown on gold surfaces were further characterized by reflection-adsorption FT-IR spectroscopy. The IR spectra observed (Figure 5a) for the "mix and match" multilayers were similar to those of metal alkanediylbis(phosphonate) films.[4e] The OH stretching vibration of the POH group at 2500−2700 and 2100−2350 cm^{-1} does not appear, indicating complete conversion of the phosphoric acid to covalently bonded zirconium phosphonate. The Zr−O stretching vibration lies at low frequency, beyond the range of the detector used. The CH$_2$ and P−O stretching bands are the
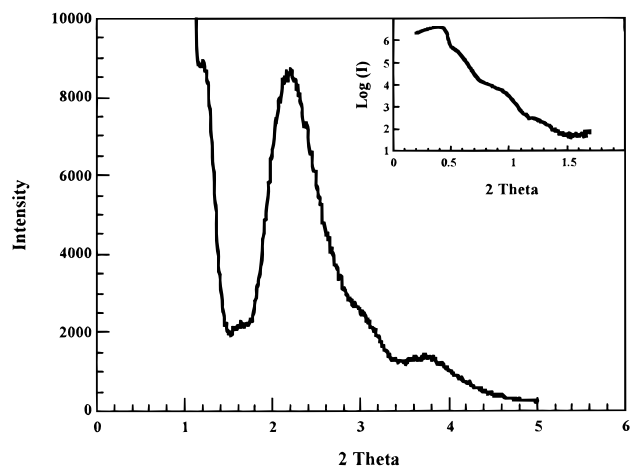
Figure 4. Thin-film X-ray diffraction pattern of Si/4-ABDMMS/[α-ZrP/Zr$_4^{8+}$/C$_{16}$BPA/Zr$_4^{8+}$]$_6$. The inset shows low-angle data (Kiessig fringes) plotted on a logarithmic intensity scale.

Figure 5. (a) Reflection–adsorption IR spectrum of [α-ZrP/Zr$_4^{8+}$/C$_{16}$BPA/Zr$_4^{8+}$]$_5$ on Au/2-MEA. (b) Reflection–adsorption IR spectrum for the same sequence, repeated 1–4 times, on Au/2-MEA, showing the C–H stretching region. The inset shows integrated peak areas vs number of C$_{16}$BPA layers.

major bands in the spectrum. The broad OH stretching vibration attributed to hydrogen-bonded water, which is usually centered at 3400 cm^{-1}, and N–H stretching modes of 2-MEA are also too weak to be observed.

The symmetric and asymmetric CH$_2$ stretching bands are found at 2855 and 2927 cm^{-1}, at slightly higher frequencies than the analogous stretching modes (2848 and 2918 cm^{-1}) in covalent Zn$_2$[O$_3$P(CH$_2$)$_{14}$PO$_3$]·2H$_2$O multilayer films.[4e] The appearance of strong symmetric and asymmetric C–H bands is consistent with C$_{16}$BPA molecules that are tilted relative to the surface normal, and possibly twisted about the P–C bond axis, as previously observed in zinc phosphonate films. The band at 1136 cm^{-1} is attributed to P–O stretching vibrations.

Two other bands at 1040 and 1230 cm^{-1} are assigned as asymmetric CH$_2$ stretching and CH$_2$ wagging modes, respectively. For one to five repeats of the α-ZrP/Zr$_4^{8+}$/C$_{16}$BPA/Zr$_4^{8+}$ adsorption sequence, the peak heights in the symmetric and asymmetric C–H stretching bands are linear with the C$_{16}$BPA layer number (Figure 5 b). These results confirm the stepwise growth of the films. The IR absorbance in the P–O stretching region, however, is not linear with the C$_{16}$BPA layer number. This may be due to the overlap of the P-O stretching peak at 1136 cm^{-1} and the two other nearby peaks at 1040 and 1230 cm^{-1}. The baseline of the peak at 1136 cm^{-1} is difficult to define because of these two nearby peaks.

X-ray Photoelectron Spectroscopy. XPS can be used to measure the surface composition and the oxidation states of elements on the surface. It is a particularly useful probe of multilayer film structure, because it offers information about the coverage and depth of cations deposited from Zr$_4^{8+}$ solutions. To distinguish zirconium in the underlying α-ZrP sheets from the Zr$_4^{8+}$ adsorbed on them, zirconium oxychloride was replaced by the analogous hafnium compound. Hafnium has similar aqueous chemistry to zirconium, and also forms Hf$_4$-(OH)$_8$(H$_2$O)$_{16}^{8+}$ (Hf$_4^{8+}$) ions at the concentrations used, typically 5 mM.[24]

XPS samples were prepared by reacting Si/4-ABDMMS/α-ZrP samples with 5 mM aqueous HfOCl$_2$·8H$_2$O for 3 h and washing with neutral nanopure water. The resulting Si/4-ABDMMS/α-ZrP/Hf$_4^{8+}$ samples were dried and XPS spectra were obtained. Two different take-off angles (20° and 75° from the surface normal) were used to derive information about the density and depth of each element in the film. The core-orbital binding energies were corrected by referencing the aliphatic C$_{1S}$ peak to 285.0 eV.[25]

XPS survey scans showed that Zr, P, Hf, Si, C, N, and O were present in the film and/or substrate. At the detection limit of the technique, no chlorine was detected, indicating that Cl$^-$ ions, which charge-compensate Hf$_4^{8+}$ ions in solution, are not present on the surface. High-resolution scans were performed to determine the relative intensities of the Zr, P, and Hf peaks in the spectrum. Normalized peak areas, A_{norm}, were calculated from eq 1, in which the atomic sensitivity factor (ASF) is an empirically determined parameter,[26] and the summation is carried out over the n different elements measured.

$$A_{norm} = \frac{area/ASF}{\sum_{j=1}^{n}(area_j/ASF_j)} \quad (1)$$

By comparing the XPS data with calculations from simple structural models, it is possible to determine the depth and coverage of Hf(IV) species on the surface. In this analysis we assume that Hf$_4^{8+}$ and Hf^{4+} are the two possible surface species, and that Hf$_4^{8+}$ has similar dimensions to Zr$_4^{8+}$. The latter is disk-shaped, approximately 9 Å in diameter and 5 Å in thickness.[19d] Three models were investigated for the Hf(IV) layer. In the first one, intact Hf$_4^{8+}$ cations lie flat on the α-ZrP surface, forming a single ca. 5 Å thick layer. In the second, the Hf$_4^{8+}$ disk stands on edge, i.e., as a Hf–O–Hf double layer on the α-ZrP sheets. In the third model the tetramer decomposes to monomeric Hf^{4+} cations, which bind to terminal oxygen atoms of the α-ZrP sheets.

(24) Mukherji, A. K. *Analytical Chemistry of Zirconium and Hafnium*; Pergamon Press: New York, 1970; Chapter 1.
(25) Beamson, G.; Briggs, D. *High Resolution XPS of Organic Polymers*; John Wiley & Sons: Chichester, England, 1992; Section 6.3, p 26.
(26) VGS 1000 manual, VG Scientific Ltd.: East Grinstead, UK, 1983.

Table 1. A_{norm} Values (in Percent) for Hf, Zr, and P,[a] from Integration of XPS Spectra, and Calculated Results from Three Structural Models for Si/4-ABDMMS/α-ZrP/Hf$_4^{8+}$

	experiment		calculation					
			Hf$_4^{8+}$ lying flat (0.016[b])		Hf$_4^{8+}$ upright (0.020[b])		Hf^{4+} dissociated (0.017[b])	
	20°	75°	20°	75°	20°	75°	20°	75°
Hf	16	40	15	24	16	21	16	26
Zr	27	22	28	24	28	26	28	24
P	59	44	57	52	56	53	56	50

[a] Only Hf, Zr, and P are considered to simplify the calculation. [b] Γ_{Hf} (atoms/Å^2).

For a given element at a depth d in the film, the contribution to the measured XPS peak intensity is given by eq 2,[27] in which I_o is the intensity obtained for the same element at the outer edge of the film. To calculate the A_{norm} values, these intensity

$$I = I_o e^{-d/\lambda} \qquad (2)$$

contributions are summed over elements at various depths, according to eq 3. Here m represents the multiplicity of atoms at a given depth. The d values are calculated by

$$A_{norm,j} = \frac{\displaystyle\sum_{j\,atoms} m_j e^{-d_j/\lambda}}{\displaystyle\sum_{all\,atoms} m_i e^{-d_i/\lambda}} \qquad (3)$$

applying experimental thicknesses of the appropriate underlying layers to each structural model, with the mean free path (λ) for all atoms fixed at an average value of 15 Å.

The coverage of Hf atoms, Γ_{Hf}, was treated as a parameter in these calculations, and a best fit to the experimental data was sought for each of the three structural models. The fraction of the surface covered by Hf$_4^{8+}$ or Hf^{4+} is the product of Γ_{Hf} (in units of atoms per Å^2), the number of Hf atoms per molecule (4 or 1), and the molecular area. The cross-sectional area of the Hf$_4^{8+}$ ion in the first (lying flat) model is about 75 Å^2, and in the second (standing up) model it is about 45 Å^2. In the third (dissociated) model, it is assumed that each Hf^{4+} ion occupies 24 Å^2, as in the α-M(HPO$_4$)$_2$·H$_2$O (M = Zr, Hf, Sn, Ti) and related metal(IV) phosphonate structures. The depth of the terminal OH groups of the α-ZrP layer was set to zero for the uncovered fraction of the surface in each model.

The results of these calculations are compared with experimental A_{norm} values for Hf, P, and Zr in Table 1. Because P atoms flank the Zr layer in the α-ZrP sheets, the calculated Zr/P ratios are rather insensitive to the model and take-off angle used. All three models show a close correspondence between observed and calculated Zr/P ratios, and therefore we may conclude that the atomic ratio is close to $^1/_2$ in the sheets. This indicates that hydrolysis of the α-ZrP sheets does not occur to any significant extent under the conditions of exfoliation or monolayer adsorption. On the other hand, A_{norm} values for Hf are sensitive to both the model and the take-off angle. At a take-off angle of 20°, where the escape depth is greatest, all three models give a good fit to the data with $\Gamma_{Hf} = 0.016-0.020$ atom/Å^2. This corresponds to one Hf$_4^{8+}$ ion per 200−250 Å^2 in models 1 and 2, or one Hf^{4+} ion per 60 Å^2 in model 3. Both coverages are considerably lower than that of Zr^{4+} in self-assembled zirconium phosphonate films, where $\Gamma_{Zr} \approx 0.04$ atom/Å^2.[4b,c] The low density of adsorbed Hf(IV) is again consistent with the greater tilt angle observed for C$_{16}$BPA layers grown on α-ZrP/Zr$_4^{8+}$. We note that both Hf$_4^{8+}$ models are consistent with charge

compensation of the α-ZrP surface, which has one ionizable PO−H group per 24 Å^2. Adsorption of one Hf^{4+} ion per 60 Å^2 (as in model 3) would overcompensate the maximum surface charge by about a factor of 2. We regard this as the strongest supporting evidence for Hf$_4^{8+}$ as the adsorbed species on α-ZrP.

All three models gave poorer fits, underestimating the contribution of Hf, to XPS data obtained at a 75° take-off angle. At glancing angles, the signals from atoms on the outer surface of the film are accentuated relative to those beneath the surface. One possible cause of this effect is underestimation of the distance between Hf atoms and the underlying α-ZrP sheets. A height error of ca. 3 Å would account for the observed discrepancy, without significantly affecting the fit to the 20° data. In any case the quality of the data is not sufficient to differentiate the three structural models.

Atomic Force Microscopy Imaging. Atomic force microscopy is a direct imaging technique that has a lateral resolution of approximately 100 Å, and a vertical resolution of ca. 1−2 Å. This technique is therefore ideal for imaging the tiling of submicron size sheets on the surface, and for accurately determining the local topography. Figure 6 shows AFM images corresponding to the step-by-step growth of a "mix and match" film on 4-ABDMMS-primed Si. Figure 6a is a topographic image of the Si/4-ABDMMS/α-ZrP surface. The α-ZrP sheets are irregularly shaped and have distinct edges, which show no signs of hydrolysis. A section analysis (Figure 7) shows that the thickness of the sheets is approximately 9 Å, consistent with the crystallographic repeat distance (7.6 Å) found in bulk α-ZrP. AFM images on a larger scanning scale show that the surface coverage is high (>90%), with small portions of the sheets overlapping each other. The surfaces of these α-ZrP sheets, however, are not perfectly flat. There are two kinds of topological features on the sheets. One is long, straight ridges which usually start at the edges of the sheets. These appear to arise from folding or rippling of the flexible sheets. The other prevalent features are irregular shaped patches about 2−4 nm height, which again may arise from puckering of the sheets. Some of these appear to coalesce into long streaks. We suspect that these "goosebumps", which are seen in both monolayer and multilayer samples, are regions in which some material is trapped beneath the α-ZrP sheet. Similar surface features have not yet been observed for other unilamellar inorganic sheets (e.g., HTiNbO$_5$, HCa$_2$Nb$_3$O$_{10}$) that we have imaged as monolayers by AFM.[28]

Once the α-ZrP monolayer is reacted with aqueous ZrOCl$_2$, a third kind of topographic feature appears (Figure 6b). The apparent lateral dimensions of these small features are 10−25 nm, which reflects tip effects. Their height, which can be measured without tip convolution artifacts, is about 2−4 nm. Interestingly, these smaller features tend to fill up the surface that is not covered by α-ZrP sheets, i.e., the area containing exposed 4-ABDMMS. They are too large to be individual Zr$_4^{8+}$

(27) Ertl, G.; Kuppers, J. *Low Energy Electrons and Surface Chemistry*, 2nd ed.; VCH: Weinheim, FRG, 1985; pp 74−79.

(28) Fang, M.; Kim, C. H.; Sutorik, A. C.; Kaschak, D. M.; Mallouk, T. E. *In Amorphous & Crystalline Insulating Thin Films*; MRS Proceeding, 1996; Vol. 446, p 337.
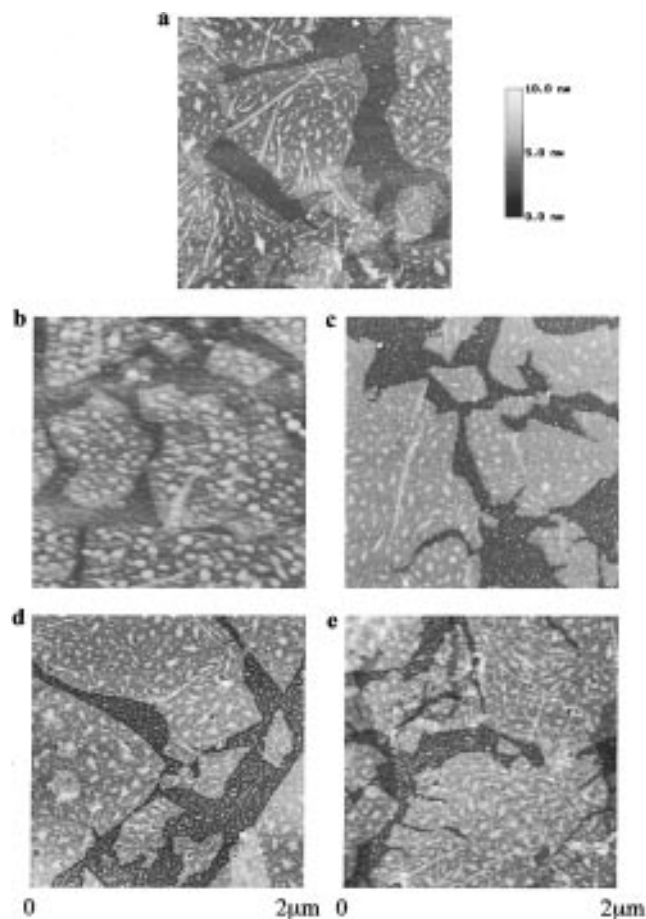
Figure 6. Tapping-mode AFM images of (a) Si/4-ABDMMS/α-ZrP, (b) Si/4-ABDMMS/α-ZrP/Zr_4^{8+}, (c) Si/4-ABDMMS/α-ZrP/Zr_4^{8+}/C_{16}-BP, (d) Si/4-ABDMMS/α-ZrP/Zr_4^{8+}/C_{16}BP/Zr_4^{8+}, and (e) Si/4-AB-DMMS/α-ZrP/Zr_4^{8+}/C_{16}BP/Zr_4^{8+}/α-ZrP.
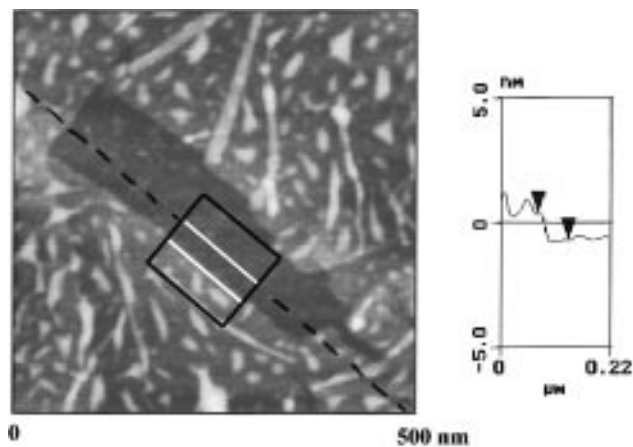

Figure 7. AFM image and line scan of Si/4-ABDMMS/α-ZrP, showing the height of the step between the α-ZrP sheet and the 4-ABDMMS-derivatized surface. The white lines within the square box correspond to lines on the surface that were averaged, and are indicated as marker arrows in the line scan. The height difference between the surface and the top of the sheet is ca. 9 Å.

cations, and the latter do not adsorb to cationic (NH_3^+-terminated) surfaces. It is possible that these small features are 2−4 nm diameter zirconium hydroxide particles present in the 5 mM $ZrOCl_2$ solution, which is somewhat sensitive to base hydrolysis. Adsorption of the C_{16}BPA layer causes no obvious changes in the surface topography, but the average height of the α-ZrP/Zr_4^{8+}/C_{16}BPA multilayer films is 35 Å relative to the surrounding 4-ABDMMS regions. The second $ZrOCl_2$

adsorption step (Figure 6d) again results in no noticeable changes in topography, except for an increase in height of the multilayer relative to the background. Finally, a second layer of α-ZrP sheets is adsorbed, resulting in the topography shown in Figure 6e. Both the first and second layers of sheets are visible in this image, and the average height difference is 45 Å, which is reasonably consistent with the 40 Å repeat distance inferred from XRD and ellipsometric data.

Related "Mix and Match" Experiments. Despite the fact that several monomeric and oligomeric cations form stable intercalation compounds with zirconium phosphate and related lamellar cation exchangers,[29] the Zr_4^{8+} and Hf_4^{8+} ions have proven to be uniquely effective in switching between covalent and ionic layer sequences. In addition to Zr_4^{8+} and Hf_4^{8+}, several divalent (Zn^{2+}, Cu^{2+}, Co^{2+}, Ca^{2+}, and Ba^{2+}) and trivalent (Al^{3+} and La^{3+}) metal salts were tested in this system. While these ions bind persistently to the C_{16}BPA surface, and can be incorporated into covalent sequences joined to ionic sequences by α-ZrP/Zr_4^{8+}/C_{16}BPA sequences, none were effective in binding α-ZrP. The α-ZrP sheets also appear to have a unique affinity for Zr_4^{8+} and Hf_4^{8+}. Preliminary experiments with $TiNbO_5^-$ and $Ca_2Nb_3O_{10}^-$ colloids, which readily form multilayer films with PAH, showed that they do not bind to the C_{16}BPA/Zr_4^{8+} surface. Again, these other lamellar colloids are easily incorporated into the ionic sections of "mix and match" sequences, but cannot be used to join covalent blocks to ionic ones. The alkanediylbis(phosphonic) acid is also a critical component of the joining sequence, since α-ZrP does not adsorb persistently to surfaces terminated by α-ZrP/Zr_4^{8+}. It appears that in this case the Zr_4^{8+} layer does not have enough excess charge to bind the anionic α-ZrP sheets. Again, this is consistent with XPS results, which showed that if the surface species is Zr_4^{8+}, its surface coverage is sufficient to compensate but not over-compensate the charge of the underlying anionc sheets.

Conclusions

Self-assembled thin films in which sequentially adsorbed ionic and covalent components have been grown on Si and Au surfaces. The three-layer adsorption sequence α-ZrP/Zr_4^{8+}/C_n-BPA acts as a bridge between the ionic and covalent parts of these assemblies. While modeling of XPS data cannot unambiguously resolve the nature of the M(IV) (M = Zr, Hf) species in the intermediate layer, the density of ions on the surface is consistent with charge compensation of α-ZrP by intact M_4^{8+} ions. Ellipsometry, X-ray diffraction, and atomic force microscopy confirm that the intermediate C_{16}BPA layer is anomalously thin, relative to layers grown in purely covalent sequences. This observation is also consistent with the lower chain density that would attend binding to Zr_4^{8+} ions, rather than dissociated Zr^{4+} at the same value of Γ_{Zr}.

The α-ZrP/M_4^{8+}/C_nBPA (M = Zr, Hf) sequence appears to be uniquely effective in joining the ionic and covalent parts of these multilayer films. It is possible that other oligomeric cations, for example oxycations of aluminium, chromium, nickel, and other elements that have been used to pillar α-ZrP[29] and smectite clays,[30] will serve the same function. Monomeric metal ions (M^{2+} and M^{3+}) appear to simply charge compensate

(29) Clearfield, A.; Roberts, B. D. *Inorg. Chem.* **1988**, *27*, 3237.

(30) (a) Burch, R.; Warburton, C. I. *J. Catal.* **1986**, *97*, 503. (b) Bartley, G. J. J.; Burch, R. *Appl. Catal.* **1985**, *19*, 175. (c) Yamanaka, S.; Brindley, G. W. *Clays Clay Miner.* **1978**, *26*, 21. (d) Clearfield, A. In *Surface Organometallic Chemistry: Molecular Approaches to Surface Catalysis*, Basset, J.-M., Ed., Kluwer, Dordrecht, 1998, pp 271−298.

the α-ZrP surface, and do not provide a stable anchoring point for C_nBPA. Despite the fact that the bridging sequence is limited at present to this one unique case, the "mix and match" method is actually quite versatile, because many different components can be included in either ionic or covalent sequences in the film. The technique thus should enable the preparation of complex surface heterostructures, which combine the fine structural control inherent in covalent metal phosphonate self-assembly with the broad compositional variety and forgiving nature of the ionic self-assembly technique.

JA972569E